Monodisperse, Micrometer-Scale, Highly Crystalline, Nanotextured Ag Dendrites: Rapid, Large-Scale, Wet-Chemical Synthesis and Their Application as SERS Substrates

ARTICLE *in* ACS APPLIED MATERIALS & INTERFACES · OCTOBER 2010

Impact Factor: 6.72 · DOI: 10.1021/am100968j · Source: PubMed

4 AUTHORS, INCLUDING:

Lei Wang
Huazhong University of Science and Techn…
301 PUBLICATIONS **5,986** CITATIONS
SEE PROFILE

Hailong Li
Chinese Academy of Sciences
45 PUBLICATIONS **1,310** CITATIONS
SEE PROFILE

Xuping Sun
Chinese Academy of Sciences
269 PUBLICATIONS **7,927** CITATIONS
SEE PROFILE

Monodisperse, Micrometer-Scale, Highly Crystalline, Nanotextured Ag Dendrites: Rapid, Large-Scale, Wet-Chemical Synthesis and Their Application as SERS Substrates

Lei Wang,[†] Hailong Li,[†,‡] Jingqi Tian,[†,‡] and Xuping Sun*[,†]

State Key Lab of Electroanalytical Chemistry, Changchun Institute of Applied Chemistry, Chinese Academy of Sciences, Changchun 130022, Jilin, China, Graduate School of the Chinese Academy of Sciences, Beijing 100039, China

ABSTRACT In this letter, we report on our interesting finding that the direct mixing of aqueous $AgNO_3$ and NH_2OH solutions at room temperature leads to rapid, high-yield production of monodisperse, micrometer-scale, highly crystalline, nanotextured Ag dendrites. The surface-enhanced Raman scattering (SERS) effect of these Ag dendrites was evaluated by using 4-aminothiophenol (*p*-ATP) as the Raman probe and the results demonstrate that they exhibit strong SERS effects.

KEYWORDS: monodisperse • nanoparticle • Ag • dendrite • wet-chemical synthesis • SERS

INTRODUCTION

During the past years, dendritic fractals of noble metal have attracted scientists' interests because of their attractive supramolecular structures that can not only provide a framework for the study of disordered systems (1) but also find important applications as catalysts (2), sensitive substrates for surface enhanced Raman scattering (SERS) (3), as well as building blocks toward superhydrophobic surface (4). As a result, much attention has been paid to their preparation and a large amount of preparative methods (2−13) have been developed, including electrochemical or electroless metallic deposition, γ-irradiated deposition, dielectric breakdown, vapor-phase polymerization, ultraviolet irradiation photoreduction using poly(vinyl alcohol) as a protecting agent, solvothermal methods using poly(vinyl pyrrolidone) as an adsorption agent and architecture soft template, ultrasonic wave-assisted hard template method, controlled seeding method, a micellar or mixed surfactant route, hydrolysis of poly(vinyl acetone)-assisted method, and using zinc microparticles suspension as a heterogeneous reducing agent in the absence of surfactant. We also developed a simple wet-chemical route for the preparation of snowflakelike dendritic nanostructures of Ag by directly mixing $AgNO_3$ and *p*-phenylenediamine aqueous solutions at room temperature (14). Unfortunately, all these above-mentioned methods suffer from more or less severe drawbacks such as special equipment required, time-consuming, unclean particle surface, and impurity of the products, which push the researchers to explore new preparative approach overcoming such limitations. More recently, Gutés et al. have fabricated Ag dendrites with a large surface area-to-volume ratio on commercial aluminum foil to produce cost-effective SERS substrates, which is based on a silver galvanic displacement process where aluminum is oxidized while silver ions are reduced (15). However, this method suffers from that it cannot produce monodispersed Ag dendrites, is time-consuming, and the reaction yield is only 40%.

In this letter, we report on our interesting finding that monodisperse, pure and highly crystalline, nanotextured Ag dendrites about several micrometers in size can be rapidly and reproducibly produced in high yield by direct mixing of aqueous $AgNO_3$ and NH_2OH solutions at room temperature. The possible dendrite formation mechanism is discussed. The influence of experimental parameters including molar ratio and concentration of the reactants and the reaction temperature on the dendrite formation is also examined and it is found that the temperature is critical to the formation of dendritic Ag. The SERS effect of these Ag dendrites was evaluated by using *p*-ATP as the model Raman probe and the results show that such Ag dendrites can effectively enhance the Raman signal of *p*-ATP. Most importantly, it suggests that the SERS signal on these particles is much stronger than that on the particles obtained by the silver galvanic displacement process (15) when exposed to similar concentrations of *p*-ATP.

EXPERIMENTAL SECTION

Ag dendrites were prepared as follows: In a typical preparation, 100 μL of 0.45 M $AgNO_3$ aqueous solution was added into 1.5 mL of 0.12 M NH_2OH aqueous solution with 4:1 molar ratio of NH_2OH to Ag under vigorous shaking at room temperature (sample 1). A large amount of precipitate

* To whom correspoandence should be addressed. Tel/Fax: (+86)431-85262065. E-mail: sunxp@ciac.jl.cn.

Received for review August 25, 2010 and accepted October 13, 2010

† Changchun Institute of Applied Chemistry, Chinese Academy of Sciences.

‡ Graduate School of the Chinese Academy of Sciences.

DOI: 10.1021/am100968j

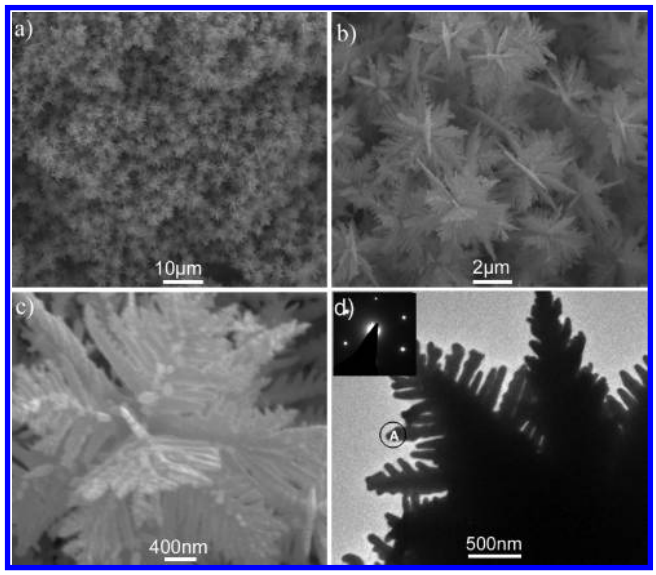

FIGURE 1. Typical SEM images of Ag particles of sample 1 (a, b, and c correspond to different magnifications); (d) the local view of one single Ag dendrite and the corresponding SAED pattern (inset).

was observed within several minutes. As-formed precipitate was washed twice with water and dispersed in water for characterization and further use. Scanning electron microscopy (SEM) measurements were made on a XL30 ESEM FEG scanning electron microscope at an accelerating voltage of 20 kV. Samples for SEM examination were made by placing a drop of the dispersion of the precipitate in water on a glass slide and air-dried at room temperature. Transmission electron microscopy (TEM) measurements were made on a Zeiss LIBRA 120 microscope operated at an accelerating voltage of 120 kV. Samples for TEM examination were made by placing a drop of the dispersion of the precipitate in water on a carbon-coated copper grid and air-dried at room temperature. X-ray diffraction (XRD) analysis was carried out on a D/Max 2500 V/PC X-ray diffractometer using Cu (40 kV, 200 mA) radiation. The sample for XRD characterization was prepared by placing some precipitate on a glass slide. X-ray photoelectron spectroscopy (XPS) analysis was measured on an ESCALAB MK II X-ray photoelectron spectrometer using Mg as the exciting source. SERS spectra were collected with a Renishaw 2000 model confocal microscopy Raman spectrometer with a CCD detector and a holographic notch filter (Renishaw Ltd., Gloucestershire, U.K.) at ambient conditions. Radiation of 514.5 nm from an air-cooled argon ion laser was used for the SERS excitation. The laser beam was focused to a spot with a diameter of approximately 1 μm using a 50× microscope objective. The data acquisition time was 30 s for one accumulation. The Raman band of a silicon wafer at 520 cm^{-1} was used to calibrate the spectrometer.

RESULTS AND DISCUSSION

Figure 1a shows the low-magnification SEM image of the precipitate of sample 1. It is clearly seen that the precipitate consists exclusively of a large quantity of micrometer-scale particles. The energy-dispersive spectrum (EDS) shows that as-formed product exclusively consists of Ag (see Figure S1 in the Supporting Information), that is, only pure and clean

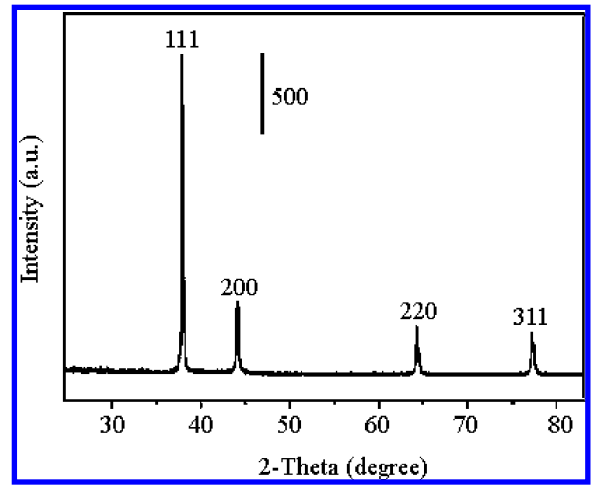

FIGURE 2. XRD pattern of the precipitate of sample 1.

Ag particles are formed. The higher-magnification SEM image of these particles shown in Figure 1b indicates that they are monodisperse and about 4.5 μm in size and dendritic in shape. A close view of one single dendrite further reveals that it consists of aggregated nanoparticles and has nanoroughened surface, as shown in Figure 1c. Figure 1d shows the local TEM view of one single Ag dendrite, further revealing its dendritic nature. The local crystalline nature of the dendrite was examined by electron beam microanalysis by TEM. It should be pointed out that the center part along each branch of the dendrite is too thick to be penetrated by the electron beam, and therefore we collected the selected-area electron diffraction (SAED) pattern recorded by focusing an electron beam on the edge of one branch (e.g., as indicated by A). The observation of a hexagonal symmetry diffraction spot pattern (Figure 1d inset) indicates that the dendrite is single crystalline (14). The crystalline nature of the bulk dendrites was further examined by XRD analysis. Figure 2 shows the XRD pattern collected. All the diffraction peaks observed can be assigned to the {111}, {200}, {220}, and {311} diffraction peaks of the cubic structure of metallic Ag, respectively, indicating that the dendrite is crystalline Ag. The fact that the intensity ratio between the {111} and {220} diffraction peaks is higher than that of the standard file (JCPDS) (5.1 versus 2.5) indicates that the dendrites are highly crystalline and abundant in {111} facets (14). It should be noted that the resulting Ag dendrites are robust enough to stand a violent sonication process, which is evidenced by the observation that the integration of each dendrite remains unchanged after a period of 30 min of sonication (see Figure S2 in the Supporting Information). We also investigated the time-dependent morphology evolution of such Ag structures by collecting SEM images with elapsed times of about 30 s, 2 min, and 10 min after the mixing of $AgNO_3$ and NH_2OH aqueous solutions (Figure 3) and found that each sample gives quite similar structures to the final products, indicating that the formation of Ag dendrites is a fast process. It should be mentioned that the Ag3d XPS spectrum of the dendrites shows two peaks at 373.7 and 367.9 eV (see Figure S3 in the Supporting Information), revealing the Ag(0) nature of the dendrites

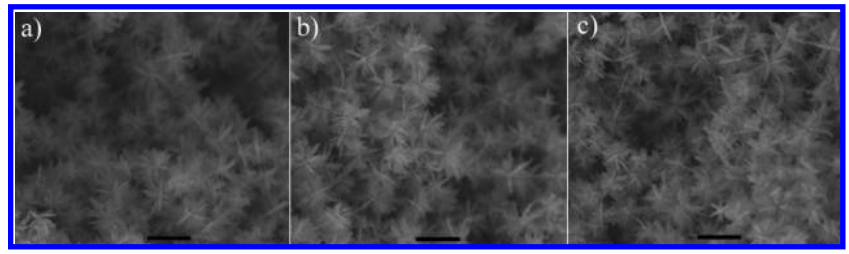

FIGURE 3. SEM images of Ag structures formed with elapsed times of about 30 s, 2 min, and 10 min after the mixing of $AgNO_3$ and NH_2OH aqueous solution (scale bar: 5 μm).

(16). It is also worth mentioning that about 98% Ag^+ is transformed into Ag dendrites, indicating this approach is high yield in nature.

The spontaneous formation of Ag dendrites can be attributed to the direct redox between NH_2OH and Ag^+. Indeed, Leopold et al. have demonstrated the formation of spherical Ag nanoparticles by chemical reduction of silver nitrate (1 mM) with $NH_2OH \cdot HCl$ at alkaline pH and at room temperature (17), the main difference between which and our present study is that the concentration of Ag^+ in our system is much higher (~28 mM). In their study, sodium hydroxide was added to $NH_2OH \cdot HCl$ solution to increase its pH above 7 before the introduction of Ag^+. After the redox reaction, however, a final pH of 7 was measured and such decrease in pH can be attributed to the release of protons during the reaction. In our study, we used NH_2OH instead of $NH_2OH \cdot HCl$ and the pH values of the reaction system were measured to be about 9.2 and 7.1, respectively, before and after the redox reaction, indicating there is almost no difference in pH between these two systems. It is well-established that an increase in concentration of the reactants leads to increased reaction rate and thus a nonequilibrium system being easily built, which is beneficial in the formation of dendrites (18). We also performed one control experiment where $NaBH_4$ was used as a reducing agent, under otherwise identical conditions used for preparing sample 1; however, only irregular Ag structures were obtained. All the above observations indicate the formation of Ag dendrites in our present study is attributed not only to the high concentration of the reactants, but to the unique nature of NH_2OH. Therefore, it is reasonable to suggest that both a rapid nucleation and growth kinetics of Ag nanoparticles and the NH_2OH molecules contribute mainly to the formation of the dendrites. It was reported that low-molar-mass additives or inorganic ions can influence crystal habit by a selective adsorption process leading to preferential growth inhibition for distinct crystal faces (19), and single crystals with complex morphologies such as flowerlike can be obtained when multiple steps are involved in such processes (20). The observation that the aggregates of Ag nanoparticles with complex, snowflakelike dendritic morphology are highly crystalline in the present study indicates that multiple steps are involved in the formation process of Ag dendrites. We speculate that the formation of Ag dendrites is accomplished by the following three steps: (1) $AgNO_3$ is rapidly reduced by NH_2OH to form Ag atoms when these two solutions are mixed together. Because NH_2OH is a strong reducing agent and $AgNO_3$ is a powerful oxidant, it is expected that all the Ag^+ ions have been completely reduced at this step, leading to highly concentrated Ag atoms. (2) Highly concentrated Ag nanoparticles are rapidly formed by an initial nucleation phase in which tiny seed Ag particles precipitate spontaneously from solution, and a subsequent growth phase in which newly formed seeds capture free Ag atoms in the solution (21). The NH_2OH may serve as an additive for the formation of single-crystalline Ag nanoparticles. (3) A crystal growth through NH_2OH-mediated aggregation of Ag nanoparticles occurs (22). Each nanoparticle can serve as an immobile "seed" in the solution. Some free nanoparticles are then launched from a random position far away and are allowed to diffuse toward the seed. Once they touch the seed, they are immobilized instantly on the empty surface of the seed, yielding an initial aggregate of Ag nanoparticles with the seed as the center and the attached nanoparticle as the arm. With elapsed time, other free nanoparticles will diffuse continually toward the aggregate and further be immobilized on the empty surface of the arm, forming a larger aggregate. This crystal growth process can be repeated until all free nanoparticles are depleted, leading to dendritic crystals. Actually, there is a mass of seeds distributed uniformly in the solution, and multiple aggregation events occur simultaneously in the respective regions of the solution. As a result, monodispersed dendrites with limited size are obtained. During the formation of aggregates, the NH_2OH molecules may dictate the oriental attachment of Ag nanoparticles, and thus highly crystalline, dendritic aggregates of Ag nanoparticles are formed finally. However, the detailed mechanism is not completely understood and requires further study.

We examined the influence of the molar ratio of the reactants on the formation of the Ag dendrites. Figure S4 in the Supporting Information shows SEM images of Ag structures obtained with varied molar ratio of NH_2OH to Ag. Under both conditions, we also obtained monodisperse Ag dendrites whose size is identical to that formed under 4:1 molar ratio (sample 1). We also found that decreased molar ratio leads to more open structures. We further investigated the influence of the concentration of the reactants on the formation of Ag dendrites. Figure S5 in the Supporting Information shows SEM images of the resulting Ag structures obtained by (a, b) increasing the concentration up to 4-fold and (c, d) decreasing the concentration down to 1/4. Again, monodisperse Ag dendrites about 4 μm in size are formed for both cases. It is observed that increased concentration leads to dendrite with thicker leaves. All these observations indicate that well-defined, monodisperse Ag dendrites can

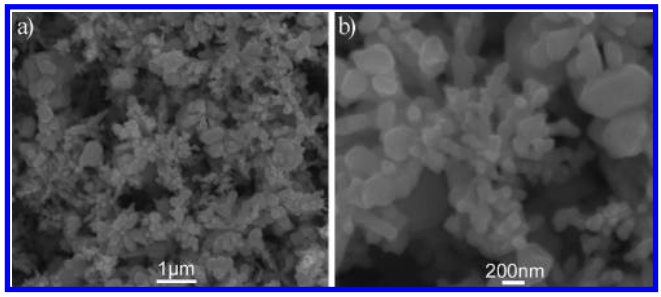

FIGURE 4. SEM images of the Ag particles obtained at 50 °C, under otherwise identical conditions used for preparing sample 1.

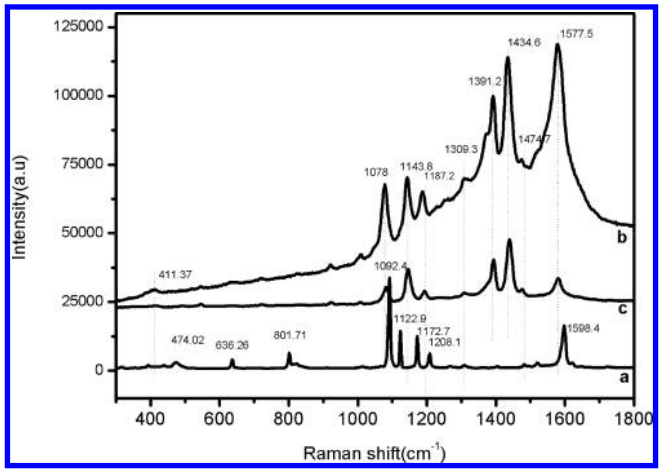

FIGURE 5. (a) Raman spectrum of solid *p*-ATP, SERS spectra of *p*-ATP (1×10^{-4} M) on Ag dendrites obtained (b) in present study and (c) by the silver galvanic displacement process.

form reproducibly under varied molar ratio and concentration of the reactants. It is worth mentioning that the use of higher temperature 50 °C only produces irregular particles (Figure 4), indicating that more fast nucleation and growth kinetics is not in favor to the dendritic shaping of Ag particles in our present system. However, the detailed growth mechanism of the well-defined Ag dendrites is not clear so far and requires further study.

Given the observation that the surface of such Ag dendrites is nanoroughed in nature, we evaluated their potential application as SERS substrates by using *p*-ATP as a model Raman probe. Figure 5 shows the Raman spectrum of solid *p*-ATP (curve a) and the SERS spectra of *p*-ATP on the Ag dendrites of sample 1 assembled on a glass slide (curve b). In one control experiment, we also collected the spectrum of the Ag dendrites in the absence of *p*-ATP and found that Ag dendrites alone can not give any Raman signals (data not shown). The normal Raman spectrum of solid *p*-ATP is similar to that reported in the literature (23). Compared to the spectrum obtained in the solid, the SERS spectrum obtained on the Ag dendrites shows distinct frequency shifts for some changes in band intensity. The ν_{CS} band shifts from 1092 cm^{-1} (curve a) to 1078 cm^{-1} (curve b), and another frequency shift from 1598 to 1577 cm^{-1} was also observed. Such observations clearly show that the −SH group of *p*-ATP makes direct contact with the Ag dendrite surface by forming a strong Ag−S bond (24). The Raman spectrum of *p*-ATP on the Ag dendrites-modified glass slide exhibited four b_2 modes at 1577.5, 1434.6, 1391.2, and 1143.8 cm^{-1} and one a_1 mode at 1078 cm^{-1}, which is quite similar to those of *p*-ATP absorbed on Ag nanoparticles (25). These two peaks at 1391.2 and 1434.6 cm^{-1} are caused by the formation of *p*,*p*′-dimercaptoazobenzene produced from *p*-ATP by selective catalytic coupling reaction on Ag surface (26). The strong SERS effects should be mainly originated from the nanogap/grooves between the nanostructures on the Ag dendrite surface (27−29). It should be pointed out that the SERS signal on these particles (curve b) is much stronger than that on the particles obtained by the silver galvanic displacement process (curve c) when exposed to similar concentrations of *p*-ATP.

To determine the enhancement effect of *p*-ATP on the assembling film quantitatively, we calculated the enhancement factor (EF) values of *p*-ATP in the assembling film using the following expression

$$EF = (I_{SERS}/N_{ads})/(I_{bulk}/N_{bulk})$$

Where I_{SERS} stands for the intensity of a vibrational mode in the SERS spectrum of *p*-ATP and I_{bulk} for that of solid sample. N_{abs} and N_{bulk} are the number of *p*-ATP molecules adsorbed on the SERS substrate and bulk molecules illuminated by the laser light to obtain the corresponding SERS and ordinary Raman spectra, respectively. *N*ads can be obtained according to the reported method (30), which is

$$N_{ads} = N_d A_{laser} A_N/\sigma$$

Where N_d is the number density of the Ag dendrites, A_{laser} is the area of the focal spot of laser, A_N is the Ag dendrites footprint area, and σ is the surface area occupied by an adsorbed *p*-ATP molecule. N_d and A_N can be obtained from the SEM images shown in Figure 1B, and A_{laser} can be obtained from the diameter of the laser spot (∼1 μm). It was reported that each *p*-ATP molecule occupies ∼0.20 nm^2, indicating that σ can be adopted as ∼0.20 nm^2/molecule (31, 32). The total number of surface adsorbed molecules (N_{ads}) within the illuminated laser spot can then be obtained at 3.08×10^6. N_{bulk} is the molecule number of the solid *p*-ATP in the laser illumination volume. In our experiment, the laser spot of 1 μm in diameter and the penetration depth (∼2 μm) of the focused laser beam are used. Taking the density of the solid *p*-ATP (1.18 g/cm^3) into account, N_{bulk} was calculated to be about 8.9×10^9 within the illuminated laser light. Considering that the intensity at 1078 cm^{-1} (curve b) and 1092.4 (curve a) was measured to be about 67786 and 33904 for SERS and ordinary Raman, respectively, the EF at the assembling Ag dendrites for the band located at 1078 cm^{-1} can be calculated to be as large as 5.78×10^3 at 514 nm excitation.

CONCLUSION

In conclusion, we develop a simple wet-chemical method for the rapid, high-yield production of monodisperse, micrometer-scale, highly crystalline, nanotextured Ag dendrites. The reaction temperature has proven to be the key

parameter to the formation of well-defined dendritic shape. The preliminary use of such Ag dendrites as effective SERS substrates has also been demonstrated. Our findings are significant for the following two reasons: (1) It provides us a new methodology for the preparation of Ag dendrites for applications (2−4). (2) Such dendrites can find new applications toward the concentrating and gravity-driven separation of biomacromolecules.

Acknowledgment. This work was supported by National Basic Research Program of China (973 Program) (No. 2011CB935803).

Supporting Information Available: EDS of the precipitate of sample 1; SEM image of the Ag structures of sample 1 after sonication for 30 min; Ag3d XPS spectrum of the Ag dendrites. SEM images of Ag dendrites obtained with 6:1 and 2:1 molar ratio of NH_2OH to Ag; SEM images of Ag dendrites obtained with 4-fold and 1/4 concentration of the reactants (PDF). This material is available free of charge via the Internet at http://pubs.acs.org.

REFERENCES AND NOTES

(1) Fleury, V.; Kaufman, J. B.; Hibbert, D. B. *Nature* **1994**, *367*, 435.
(2) Chimentão, R. J.; Kirm, I.; Medina, F.; Rodríguez, X.; Cesteros, Y.; Salagre, P.; Sueiras, J. E. *Chem. Commun.* **2004**, 846.
(3) Liang, H.; Li, Z.; Wang, W.; Wu, Y.; Xu, H. *Adv. Mater.* **2009**, *21*, 12.
(4) Zhang, X.; Shi, F.; Yu, X.; Liu, H.; Fu, Y.; Wang, Z.; Jiang, L.; Li, X. *J. Am. Chem. Soc.* **2004**, *126*, 3064.
(5) Zhang, X.; Shi, F.; Yu, X.; Liu, H.; Fu, Y.; Wang, Z.; Jiang, L.; Li, X. *J. Am. Chem. Soc.* **2004**, *126*, 3064.
(6) Wang, S.; Xin, H. *J. Phys. Chem. B* **2001**, *104*, 5681.
(7) Niemeyer, L.; Pietronero, L.; Wiesmann, H. J. *Phys. Rev. Lett.* **1984**, *52*, 1033.
(8) Selvan, S. T. *Chem. Commun.* **1998**, 351.
(9) Zhou, Y.; Yu, S.; Wang, C.; Li, X.; Zhu, Y.; Chen, Z. *Adv. Mater.* **1999**, *11*, 850.
(10) Dick, K. A.; Deppert, K.; Larsson, M. W.; Martensson, T.; Seifert, W.; Wallenberg, L. R.; Samuelson, L. *Nat. Mater.* **2004**, *3*, 380.
(11) Song, Y.; Yang, Y.; Medforth, C. J.; Pereira, E.; Singh, A. K.; Xu, H.; Jiang, Y.; Brinker, C. J.; van, Swol.; Shelnutt, J. A. *J. Am. Chem. Soc.* **2004**, *126*, 635.
(12) Wu, W.; Pang, W.; Xu, G.; Shi, L.; Zhu, Q.; Wang, Y.; Lu, F. *Nanotechnology* **2005**, *16*, 2048.
(13) Wen, X.; Xie, Y.; Mak, W. C.; Cheung, K. Y.; Li, X.; Renneberg, R.; Yang, S. *Langmuir* **2006**, *22*, 4836.
(14) Sun, X.; Hagner, M. *Langmuir* **2007**, *23*, 9147.
(15) Gutés, A.; Carraro, C.; Maboudian, R. *J. Am. Chem. Soc.* **2010**, *132*, 1476.
(16) Sun, X.; Dong, S.; Wang, E. *Macromolecules* **2004**, *37*, 7105.
(17) Leopold, N.; Lendl, B. *J. Phys. Chem. B* **2003**, *107*, 5723.
(18) Nittmann, J.; Stanley, H. E. *Nature* **1986**, *321*, 663.
(19) Adair, J. H.; Suvaci, E. *Curr. Opin. Colloid Interface Sci.* **2000**, *5*, 160.
(20) Cölfen, H.; Qi, L.; Mastai, Y.; Börger, L. *Cryst. Growth Des.* **2002**, *2*, 191.
(21) deMello, J.; deMello, A. *Lab Chip* **2004**, *4*, 11N.
(22) Cölfen, H.; Mann, S. *Angew. Chem., Int. Ed.* **2003**, *42*, 2350.
(23) Wang, Y.; Chen, H.; Dong, S.; Wang, E. *J. Chem. Phys.* **2006**, *124*, 074709−1.
(24) Wei, G.; Wang, L.; Liu, Z.; Song, Y.; Sun, L.; Yang, T.; Li, Z. *J. Phys. Chem. B* **2005**, *109*, 23941.
(25) Guo, S.; Dong, S.; Wang, E. *Cryst. Growth Des.* **2009**, *9*, 372.
(26) Fang, Y.; Li, Y.; Xu, H.; Sun, M. *Langmuir* **2010**, *26*, 7737.
(27) Moskovits, M. *Rev. Mod. Phys.* **1985**, *57*, 783.
(28) Xu, H.; Bjerneld, E. J.; Käll, M.; Börjesson, L. *Phys. Rev. Lett.* **1999**, *83*, 4357.
(29) Xu, H.; Aizpurua, J.; Käll, M.; Apell, P. *Phys. Rev. E* **2000**, *62*, 4318.
(30) Orendorff, C. J.; Gole, A.; Sau, T. K.; Murphy, C. *J. Anal. Chem.* **2005**, *77*, 3261.
(31) Kim, K.; Yoon, J. K. *J. Phys. Chem. B* **2005**, *109*, 20731.
(32) Kim, K.; Lee, H. S. *J. Phys. Chem. B* **2005**, *109*, 18929.

AM100968J